THE RANGE RESOLUTION OF A GUIDANCE INTEGRATED FUZE RADAR PROJECT

by

Cory R. Tonks

A report submitted in partial fulfillment
of the requirements for the degree

of

MASTER OF SCIENCE

in

Electrical Engineering

Approved:

Dr. Jacob Gunther Major Professor	Dr. Randy Jost Committee Member

Dr. Reyhan Baktur
Committee Member

UTAH STATE UNIVERSITY
Logan, Utah

2009

Abstract

The Range Resolution of a Guidance Integrated Fuze Radar Project

by

Cory R. Tonks, Master of Science

Utah State University, 2009

Major Professor: Dr. Jacob Gunther
Department: Electrical and Computer Engineering

The paper explains a single phase of the guidance integrated fuze (GIF) test arena project. The project phase demonstrates how collected in-phase and quadrature-phase components of a radar return signal determine the range resolution of the guidance integrated fuze subsystem and showing this subsystem operates within proper parameters. The data validates the accuracy of the test set up, the usefulness of the new facility, and demonstrates the ability to qualify a radar for this type of system.

(47 pages)

To my wife and kids for supporting me in all my goals of life and happiness.

Acknowledgments

I am thankful to the faculty and staff at Utah State University and the people at NAWCWD who assigned me to this project along with those I worked with:

Dr. Jacob Gunther, Utah State University (Committee Chair)

Randy Jost, Utah State University (Committee Member)

Dr. Reyhan Baktur, Utah State University (Committee Member)

Dr. Scott Budge, Utah State University

May Lee Anderson, Utah State University

Gene Gibson, Branch Head, NAWCWD

Dr. Curtis Kidner, Project Lead, NAWCWD

David Saunders, NAWCWD

Kevin Tajii, NAWCWD

Jacey Morrine, NAWCWD

Susan Read, NAWCWD

Deborah Tonks, Editor

Cory R. Tonks

Contents

List of Tables

List of Figures

Chapter 1

Introduction

1.1 Missile Systems

The Naval Air Warfare Center Weapons Division (NAWCWD) at China Lake, California ensures the quality of naval air systems for the U.S. Navy [1]. Some examples of naval air systems are aircrafts, missiles, and air traffic control systems. Several subsystems exist within each one of these major systems. All of these subsystems working together enable the system to achieve its functional goals. A typical missile consists of five major subsystems or sections: seeker, guidance, fuze, warhead, and propulsion [2]. Each section accomplishes specific functions.

1.1.1 Seeker

The seeker section of a missile detects targets using a sensor designed to detect specified signals. Infrared radiant power, amplification modulation (AM) radio [3], frequency modulation (FM) radio, and phase modulation (PM) radio signals [4] are a few examples of signals. Sensors range from a vast quantity of devices such as infrared cameras, radars, or other devices that can detect a specific characteristic of a target. An accurate analogy of this would be that the seeker is the eyes of the missile.

1.1.2 Guidance

Continuing with the analogy, the literal brain of the missile is the most complicated section of the missile, the guidance system. This section controls the missile's flight, interprets inputs from the seeker section or other communication systems such as the global positioning system (GPS). The guidance system responds to these inputs by sending control commands to the other subsystems of the missile. The guidance computer uses various

computer programs and mathematical techniques to optimize the command in order to enhance missile performance. These techniques are called control algorithms. An example of a control algorithm is Kalman Filtering [5]. A Kalman Filter is used to optimize a system's performance given that input to the system is a random gaussian process [6]. The Kalman Filter, or other control algorithm, enables the missile to reach its goal or continue flying until the missile reaches maximum flight range.

1.1.3 Fuze

After launch, the fuze section detects how close the missile comes to an object or target using a small radar. This is known as a proximity fuze system. The proximity fuze's radar radiates a signal through a transmit aperture until the missile intercepts an object or gets close enough for the radar to receive a return signal through the return aperture. If a return signal is received, the fuze sends a detonation signal to the warhead section. Two facts about proximity fuze radars need mentioning here. An effective proximity fuze must orient the transmit aperture to the correct forward looking angle. The angle is dependant on the average flight speed of the missile. If the angle is miscalculated, the missile will detonate at the wrong time. The other fact is that traditional proximity fuze radars can only detect objects in the radar's near-field region. Other types of fuzes include contact fuze and delay contact fuze. These contact fuzes are designed for bombs and integrated into some missiles [7]. Missiles designated to explode after launch are equipped with contact fuzes.

1.1.4 Propulsion and Warhead

The other sections, the propulsion and warhead, have very basic functions. The propulsion section ignites materials called propellants that accelerate the missile to flight speeds. This function maintains flight dynamics such as speed, lift, altitude, and direction. When all propellant material is burned, the missile has reached its maximum flight range. Once it has reached its destination, the warhead section waits for a detonate command for the fuze and ignites explosives in an attempt to destroy a target.

1.1.5 Missile Summary

All of these sections communicate among one another in order for the missile to perform at a required level of success. This paper focuses on a particular type of subsystem for a missile, a guidance integrated fuze (GIF). The guidance integrated fuzing subsystem, a part of a particular missile, has a guidance system and fuze system combined into one system [8]. This means the guidance system is also the fuze section that sends the detonate signal to the warhead section.

1.2 Radar and Radar Terminology

1.2.1 Radar

In order to understand radar data collection process for the GIF project, a list of terms must be understood. The word "radar" is an acronym for radio detection and ranging. This means a radar system senses reflected electromagnetic or radio waves which are emitted from a radio transmitter [9]. Radars are classified into two types, one-way radar and two-way radar. One-way radar performs the same function as a radio. A transmitter device sends an electric waveform into a medium, like the atmosphere. A receiving device detects the transmitted electric waveform. An example of two-way radar is like a person screaming at a wall close enough to have the sound wave from their voice reflect an echo off the wall and then have it heard a short time later [10]. Now, if the sound wave is replaced by an electric wave or waveform, radar is created. The important part of this process is the echo. An echo identifies an object some distance away from the initial wave by reflecting back towards the transmitter or person screaming. This echo, often called the return signal, is the basis of two-way radar. Throughout the rest of this paper, two-way radar and radar are synonymous. Radar requires an electromagnetic wave sensor called antennas that listens for return signals.

1.2.2 Radar Regions

The radar regions are defined as near-field or Rayleigh region, resonance or Mie region,

and the far-field or optics region [11]. The near-field region starts from the center of the target to a distance of $\frac{2\pi r}{\lambda} < 1$ where r is the radius of a sphere having an equivalent radar cross-sectional (RCS) area as the object and λ is the wavelength of the transmitted frequency. It is hard to discern object variations in this region as the RCS measurement raises linearly to the fourth power of the sphere radius until it approaches the resonance region. The resonance region is defined from $1 < \frac{2\pi r}{\lambda} < 10$. This region has a resonating curve due to a property called creeping waves. These waves actually creep around the object and transmit in the same direction of the secular reflections. This causes a constructive and destructive effect to the return signal at every half of a wavelength. The far-field region is defined as $\frac{2\pi r}{\lambda} > 10$. In this region, the constructive and destructive have an insignificant effect on the RCS measurements, making it easier to discern object variation in this region. Figure 1.1 illustrates this concept graphically [12]. Figure 1.1 shows a target's RCS is equivalent to an a sphere and how each radar region is broken down as functions of cross-sectional area and wavelength were k equals $\frac{2\pi}{\lambda}$, a is the radius from the center of the target or sphere, and σ is equal to πa^2.

1.2.3 Radar Cross-Section Measuring

Certain radar systems are able to detect objects long distances away from the transmitter. A lot of research has been done to classify objects that the radar detects by measuring the return signal which is proportional to the radar cross-sectional area at a given distance away. The RCS area is equal to the equivalent area of an isotropic object. Isotropic means an object radiates electromagnetic waves the same in all directions [13]. RCS devices are used to calibrate the accuracy of a radar system.

In 1964, W. E. Blore did a series of experiments to classify the RCS area of ogives, double-rounded cones, cone spheres, and double-backed cones at various field regions, and orientation angles to find the cross-section area of these objects [14]. These were compared to predicted values by Kennaugh and Moffatt [15]. Even though the results were compared to Kennaugh and Moffat, Blores found significant difference. This led to many follow-on studies like the Ohio State University Electro-Science Laboratory study on classification

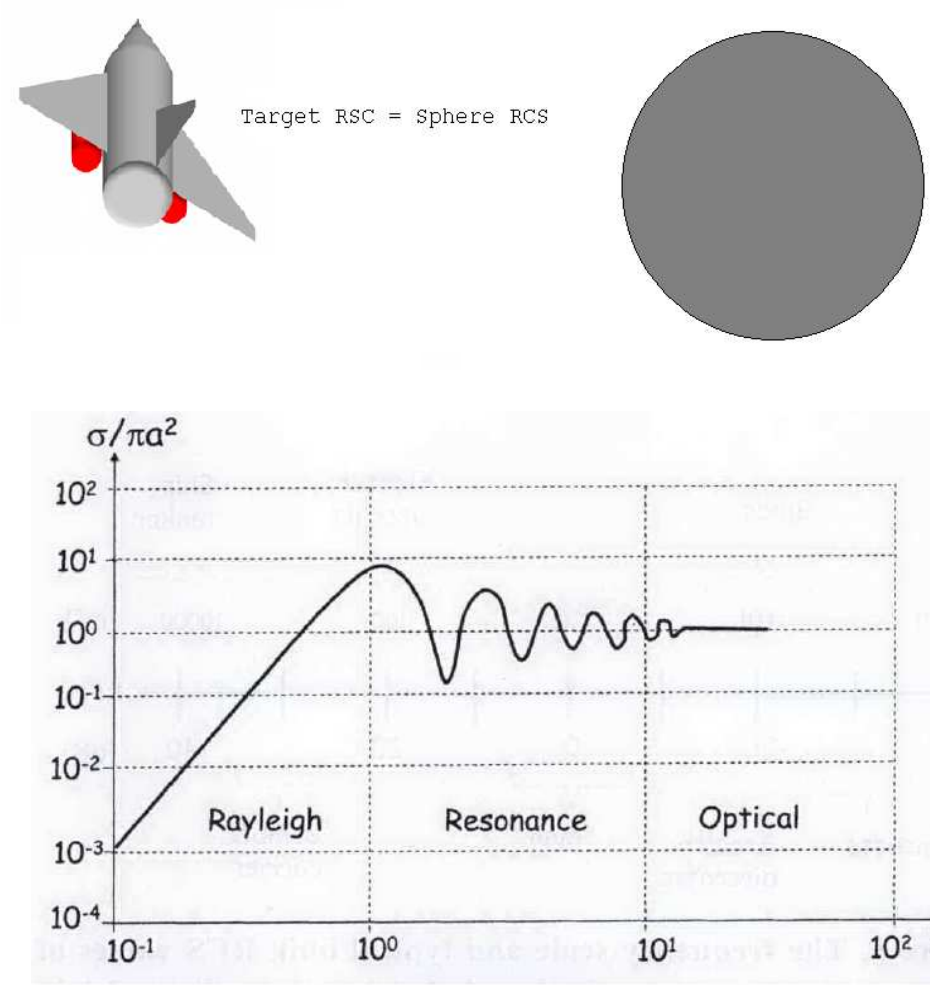

Fig. 1.1: Diagram of equivalent RCS and regions defined as wavelength verse area

techniques by Chen and Walton in 1986 [16]. This experiment's main emphasis on measuring radar signals in the resonance region to find the shape of objects. This study highlights backscattering from the resonance region from creeping waves, a factor in determining the type of object in the field of view. However, this particular experiment used the resonance-region for 1.0 to 20.0 MHz. The frequency range of the GIF project was performed in a much higher radio frequency (RF) band.

Along the lines of a military project, at the University College of Swansea, in 1993 McCowen, Macnab, and Towers tested the radar attenuation of material against a bistatic radar transmitting and receiving in the resonance region [17]. This experiment determined that the thickness of the radar attenuation material is directly related to the return signal, using the finite element method to calculate signal return from a transverse-electric (TE) and transverse-magnetic (TM) wave. This is very useful, mainly for military applications and educational purposes.

Further research of Mie scattering experiments include the Veremey and Mittra paper (1998) describing the use of a cavity-backed aperture (CBA) to collect RCS measurement [18]. The CBA was chosen because of its sensitivity and its unique resonance characteristics. By studying these characteristics, they were able to parameterize some effects of objects in the resonance region with a highly sensitive aperture. Their main objective was to test the effectiveness of a super directive CBA array.

Recognizing resonance characteristics are important when dealing with object detection in the resonance range. It enhances the radar system's ability to ignore false detections and allows an analyst to understand the data from the system.

1.3 The Guidance Integrated Fuze Project

What makes GIF an important research project? Recall the two facts about a fuze in sec. 1.1.3 of this paper. What if the missile is going so fast the forward-looking angle of the proximity fuze is just a few degrees off the nose of the missile? The idea of GIF has been around for a while as stated in "Seeker-Optimized Guidance Integrate Fuzing" [19] by Chopper and company, but there has not been a test arena developed to support massive

testing of this design. Adding a fuze algorithm to the guidance system makes one fact about proximity fuzes different than stated in sec. 1.1.3. This will force a fuze radar to operate in the radar's far-field region. This also means that the detonate command will not be given when there is something in the fuze's field of view making the other fact about proximity fuzes in sec. 1.1.3 different. A Kalman Filter or another algorithm is needed to determine when to give the detonate command or time to detonate (TTD) should be executed.

Prior research has been done on the subject of guidance integrated fuzing. The proposal written by S. Ghaleb and company about guidance integrated fuzing [20] discusses the feasible to build and test GIF at NAWCWD. This document also discusses the problems associated with this advanced type of fuzing. Ghaleb goes into great detail about Kalman filtering, simulations, and testing criteria for the seeker. Two other papers by Chopper and Jaeger talk about simulated results of a modeled GIF [21, 22]. The test data presented in Chopper and Jaeger found that the results meet the requirement of the models simulation. Lastly, the final paper discusses GIF as an integrated guidance fuze (IGF) by Z. Wang, W. Li, and N. Fan [23]. Their simulation results concluded that an IGF or GIF decreases the miss distance between the missile and the target. However, the missile's effectiveness depends on the performance parameters of the warhead. These parameters include warhead blast acceleration and blast pressure on the target.

The purpose of this paper is to report on the analysis of the collected I/Q data from each test and to validate results using numerical methods to determine if the radar operates with a high range resolution in the resonance region as described in sec. 1.2.2. How was this done? Does the I/Q signal in the resonance region reveal any phenomenon or identification information about the complex object or the radar cross-section? A later chapter discusses the project's findings. Whatever objects the radar detects need to be identifiable and locatable. Determining these facts about the object will reduce the amount of collateral damage in warfare. This will also lead to research in being able to distinguish targets as a friend or enemy. Determining if the radar has a high resolution is just one step to accomplishing this goal. This will also lead to more engineering and building of

safer weapons and aircraft identification databases, including unmanned systems and small commercial aircrafts. But before this, thorough analysis of the data must determine if the target or object is tracked in, or at, the resonance region boundaries.

1.4 Fuze Testing and the Naval Air Warfare Center Weapons Division

The facility at NAWCWD provides the ability to use high fidelity radar engagement models by reducing noise in testing environments and increase arena size for conducting near full-scale simulations. The function of the facility is to simulate the length of time that a fuze interacts with an object during a fly by. This provides the ability to test a large array of radars against any physical model. Currently the facility uses aircraft, vehicles, and other objects of interest for testing weapon fuzes. The fuze is mounted on a moveable transporter sled and autonomously placed in pre-specified test ranges from an object. The objects hang from various altitudes above the floor, positioned either left or right of the radar, and rotated to various orientation angles in the pitch and yaw axis of an object. The testing has validated many warhead fuzes in the Navy's inventory. A standard fuze test operates as follows.

1. The object is placed in the arena.
2. The transporter sled with the fuze radar is placed in a fixed range gate or initial position.
3. The object is then oriented into a test position of interest.
4. Data collection devices start recording.
5. The fuze radar is activated.
6. The sled moves at a relative trajectory velocity toward the object until the fuze sends a detect command or maximum range is achieved.
7. Data collection computers and storage devices record test data for data processing.
8. The fuze radar is turned off and reset.

9. The transporter sled is brought back to the initial position.

10. Steps 3 through 9 are repeated until the testing of the fuze radar against the test object is complete.

11. Test and systems engineers process and analyze data.

1.5 Project Work Summary

Several steps were taken in addressing the issues of this project. Work began by assigning experienced engineers and technicians parts of the project. Learning how to make the transporter sled system operate, collecting radar return signal data at various detection ranges, frequencies, and object orientations using a Pseudo-Random Bi-phase Modulation radar system took time to sort out. First, computer programming had to be done. The control computer needed to understand how the transporter sled communicated the sled's current position. After some research and help, LABView was integrated into the control computer. This program evolved into the test control program that sends commands to all of the devices and equipment for the test arena. Then the Pseudo-Random Bi-phase Modulation radar was integrated onto the transporter sled with the control program. Newer control devices needed to be integrated into the test equipment to increase sensitivity and control new function included with the new radar. The devices control the frequency sweeps, collection of radar data, sled positioning, collection of sled position, and sled speed. The different calibration scenarios were a single calibration sphere, triple calibration spheres, a single trihedral, and triple trihedrals. These calibration runs gave the information needed to collect the in-phase and quadrature-phase (I/Q) radar data. The data was processed using mathematical techniques to determine characteristics about the radar. This paper only contains the different trihedral runs.

The arena's size limit forces testing of sensors to use scaled targets. Depending on the radar's operating frequency and test requirements, models are scaled to smaller sizes to increase range for measuring signal returns in different radar regions. This scaling eliminates

complex calculations that take near-field measurements and translate them to far-field estimations. This project made the arena's range equivalent to 2400 feet, about a half-mile, by using tenth-sized models. Increasing the equivalent range allows the testing to begin in the far-field region and move the radar into the resonance region [24].

1.6 Chapter Summary

The facility collected radar data for guidance integrated fuzing missile systems. The rest of the paper addresses the data processing techniques by explaining the basis of the equations used to analyze the data, interpolated data calculations, and the results found. The process of explaining the calculation and the analysis of the collected return signals at various frequency sweeps and ranges against simple objects accomplishes the goal of this project. This technology will help NAWCWD identify objects that are actual threats and help to save the lives of innocent people while increasing the testing capabilities.

Chapter 2

Overview of Radar Equations and I/Q Components

2.1 Developing the Radar Equation

2.1.1 Introduction to Antennas

Section 1.2.1 states that a radar system traditionally needs an antenna. An antenna is the preferred aperture used for radiating or receiving [electromagnetic] waves [25]. The waves can have properties for two types of fields, the electric field, $\vec{E}$, and magnetic field, $\vec{H}$, whose units are in volts per meter and amperes per meter, respectively [26]. These fields define many of the parameters of classifying antennas, which include, for example, radiation intensity, directivity, radiation power density, gain, and efficiency [27].

2.1.2 Radiation Power Density and Radiant Power

Given an electromagnetic wave, what is the power associated with that wave? The quantity used to describe radiation power density of the wave is the instantaneous Poynting vector [28]

$$\vec{W} = \vec{E_i} \times \vec{H_i}, \tag{2.1}$$

where $\vec{W}$ is the instantaneous Poynting vector in Watts per square meter, and $\vec{E_i}$ and $\vec{H_i}$ are the instantaneous electric and magnetic fields, respectively. Since $\vec{W}$ is a power density, finding the total power vector equals the power density normal vector integrated over the entire closed surface.

$$\vec{P} = \oint \oint \vec{W} \vec{n} da, \tag{2.2}$$

where $\vec{P}$ is the instantaneous total power in Watts and da is an infinitesimal area of the closed surface in square meters. Balanis suggested that in order to analyze these waveforms,

the next step is to find the average power density obtained integrating the instantaneous Poynting vector over a wave cycle or period and dividing by the time elapsed for the cycle to complete. The complex form of $\vec{E}$ and $\vec{H}$ relate to the instantaneous counterparts as follows:

$$\vec{H}_i(x,y,z;t) = Re[\vec{H}(x,y,z)e^{j\omega t}], \tag{2.3}$$

$$\vec{E}_i(x,y,z;t) = Re[\vec{E}(x,y,z)e^{j\omega t}]. \tag{2.4}$$

Now substitute (2.3) and (2.4) into (2.1), the following is determined,

$$\vec{W} = \frac{1}{2}Re[\vec{E} \times \vec{H^*}] + \frac{1}{2}Re[\vec{E} \times \vec{H}e^{j\omega t}]. \tag{2.5}$$

Since the first term is not time varying and the second is twice the given frequency, the time average Poynting vector is:

$$\vec{W_{av}}(x,y,z) = \frac{1}{2}Re[\vec{E} \times \vec{H^*}]. \tag{2.6}$$

Relating equations (2.6) to (2.2), the average power P_{av} in an antenna is obtained, which is also the radiated power P_{rad}.

$$\vec{P_{rad}} = \vec{P_{av}} = \oint \oint \vec{W_{av}}\vec{n}da \tag{2.7}$$

2.1.3 Radiation Intensity

Balanis goes on in *Antenna Theory* [29] to define the radiation intensity as the power radiated from an antenna per unit solid angle. From the pervious section, power radiated density relates to radiation intensity as follows:

$$U = r^2\vec{W_{av}}, \tag{2.8}$$

where radiation intensity U is in Watts per unit solid angle and the range r is in meters. Now relate eqs. (2.8) to (2.7) and the following is determined,

$$\vec{P_{rad}} = \oint \oint U d\Omega, \tag{2.9}$$

where $d\Omega$ is an very small element of the solid angle. If the source is a point source, meaning the radiation intensity is free of all angular dependencies, the equation changes to:

$$\vec{P_{rad}} = \oint \oint U_o d\Omega = U_o \oint \oint d\Omega = 4\pi U_o, \tag{2.10}$$

or

$$U_o = \frac{\vec{P_{rad}}}{4\pi}. \tag{2.11}$$

2.1.4 Directivity, Efficiency, and Gain

Directivity puts radiation source in perspective. In *Antenna Theory* [30], Balanis states the directivity of a non-isotropic source is equal to the radiation of its maximum radiation intensity over the radiation intensity of an isotropic source. In this definition lies a term "isotropic" meaning the response of a material to an electric field vector $[\vec{E}]$ is the same in all directions [31]. The same applies to the magnetic field vector, $\vec{H}$, due to the fact that both are related through eq. (2.1) to radiation intensity. The material can be an antenna, a fiber optic cable or some unknown aperture that radiates the power isotropically.

Directive gain is similar to directivity except it is not direction dependant [32]. Directive gain equated to the following ratio or eq. (2.12),

$$D_g = \frac{U}{U_o} = \frac{4\pi U}{\vec{P_{rad}}}, \tag{2.12}$$

where 4π relates to the point source unit solid angle of the antenna, making the directive gain dimensionless.

Efficiency describes the losses associated with connecting the antenna to a system and the structure of the antenna itself. Shown later, miscalculation of efficiency could lead to a

system not meeting performance requirements and engineering change proposals that add cost to system development. Balanis states in *Antenna Theory* [33] the efficiency calculations break down into two groups, reflection efficiency, and antenna radiation efficiency, reflection efficiency determined by the antenna input impedance and the transmission line characteristic impedance. To find antenna input impedance, computational methods, such as method of moments, are used to determine this value [34, 35]. Antenna radiation efficiency is determined experimentally. The total efficiency of an antenna is the product of the two groups,

$$e_t = e_r e_{cd}, \tag{2.13}$$

where e_t is the total efficiency of the antenna or radiating material, e_r is the reflection efficiency, and e_{cd} is the antenna radiation efficiency. Reflection efficiency is determined by eq. (2.14).

$$e_r = 1 - \Gamma, \tag{2.14}$$

where Γ equals

$$\Gamma = \frac{Z_{in} - Z_o}{Z_{in} + Z_o}, \tag{2.15}$$

and where Z_{in} is the antenna input impedance and Z_o is the transmission line characteristic impedance.

Directive gain and efficiency create the parameter of gain. The amount of gain is proportional to the increase in output power. Transmitted signals travel farther by pointing the antenna in the direction of maximum directivity. Gain is the product of efficiency and directive gain [32, 36].

$$G = eff \times D_g \tag{2.16}$$

This quantity helps engineering design radars to perform at peak conditions given boundary conditions, such as size and available power.

2.1.5 Antenna Summary

The combination of these parameters characterize the parts of the radar system. The radar system and operational requirements determine type and parameters of the antenna.

2.2 Defining the Radar Equation

The antenna parameters defined above determine how much signal strength is transmitted and received. This begins the development of the radar equation. The radar equation is a ratio of power received given power transmitted, antenna gains, transmitted frequency, and radar cross-section.

2.2.1 Cross-Sectional Area

The initial transmitted wave propagates or radiates away from the antenna through space in the direction the antenna was pointed. When the initial wave contacts the surface of an object, that object does three things to the wave. The object reflects, absorbs, and refracts or transmits the incident wave depending of the material composition of the object [37]. The energy that returns to the receiving antenna is the scatter power density. The scatter power density is described by eq. (2.17).

$$\vec{W_s} = \lim_{R \to \infty} [\frac{\vec{W_i}\sigma}{4\pi R^2}], \tag{2.17}$$

where R is the range from the antenna to the object, $\vec{W_i}$ is the incident wave power density, $\vec{W_s}$ is the scatter wave power density, and σ is the surface area that reflects the power to the radar receiver [38–40]. Rearranging the equation gives a solution or definition to what radar cross-section is mathematically,

$$\sigma = \lim_{R \to \infty} [4\pi R^2 \frac{\vec{W_s}}{\vec{W_i}}]. \tag{2.18}$$

2.2.2 The Radar Equation

Describing the radar's return signal derives the radar equation. The power captured

by the object's cross-sectional area exposed to the incident power density or transmitted power density,

$$P_c = \sigma \vec{W}_t = \sigma \frac{P_t G_t}{4\pi R^2}, \tag{2.19}$$

where P_c is the captured power, P_t is the total transmitted power from the antenna, G_t is the gain of the transmitting antenna, W_t is the transmitted power density from the antenna and R is the range to the target [39]. A new way to calculate power density can be seen from this eq. (2.20). The scatter power density is, therefore, the captured power divided by the point source solid angle times the range squared back to the receiving antenna.

$$\vec{W}_s = \frac{P_c}{4\pi R^2} = \sigma \frac{P_t G_t}{(4\pi R^2)^2} \tag{2.20}$$

The power received by the receiver is the product of the effective area of the antenna or aperture and the scattered power density. The effective area is the product of the aperture gain and the wavelength per solid beam angle. For a point source, the following is concluded [41]:

$$A_r = G \frac{\lambda^2}{4\pi}. \tag{2.21}$$

The product of eqs. (2.20) and (2.21) gives the radar equation.

$$P_r = \frac{P_t G_t G_r \lambda^2 \sigma}{(4\pi)^3 R^4}, \tag{2.22}$$

where P_r is the received reflected power, P_t is power transmitted in watts, G_t is the transmitting antenna gain, G_r is the receiving antenna gain, λ wavelength of signal in meters, σ is target radar cross section in square meters and R is the range in meters [42].

This equation only tells the designer how much power is returned to the receiver. The equation does not describe the characteristics of the signal. A radar receiver is the only instrument that can interpret the signal. The type of receiver for the project came equipped with an I/Q demodulator.

2.3 I/Q Components

In-phase and quadrature-phase components are, respectively, the real and imaginary parts of the return signal. RCS data is a ratio of the scatter field and the initial field at the object, the signal we receive is much smaller than the transmitted signal of the radar. There have been many radar designs to help boost these signals. One way is to use continuous wave (CW) radar. This type of radar is part of the radar used to take scatter measurements for the project. CW radar can have an in-phase and quadrature-phase (I/Q) demodulator. Figure 2.1 is a common block diagram of an I/Q demodulator [43]. In figure 2.1, IF is the intermediate frequency signal, A/D means analog-to-digital, and $COHO$ is a Coherent Oscillator.

I/Q demodulation converts the intermediate frequency of a receiver into a complex representation, $I + jQ$ centered at zero frequency. Given intermediate frequency signal, eq. (2.23) is a mathematical representation of this signal split and fed into a pair of mixers or analog multipliers [44].

$$V_{IF} = A_s \sin(\omega t + \theta) \tag{2.23}$$

The local oscillators of the mixers are fed by the COHO as a reference signal. This signal is represented by the following equation:

$$V_{COHO} = A_r(\sin(\omega t) + j\cos(\omega t)). \tag{2.24}$$

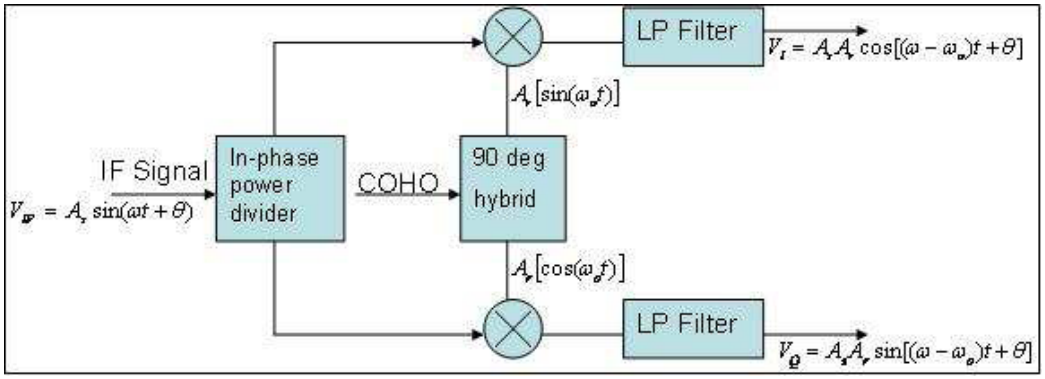

Fig. 2.1: I/Q demodulator.

Ignoring insertion losses due to the IF split the complex representation of the output is given by

$$V_{IF}V_{COHO} = \frac{A_s A_r}{2} e^{j|(\omega-\omega_o)t+\theta|} - \frac{A_s A_r}{2} e^{j|(\omega+\omega_o)t+\theta|}. \tag{2.25}$$

The ideal low-pass filter rejects the second term in eq. (2.25) producing:

$$V_I + jV_Q = \frac{A_s A_r}{2} e^{j|(\omega-\omega_o)t+\theta|}. \tag{2.26}$$

This process breaks the return signal into real and imaginary parts. This is done to use mathematical techniques for creating radar images of the objects using Fourier transforms other techniques explained in the next section.

2.4 I/Q Data Processing

2.4.1 General Explanation of Mathematics

This section explains the general approach of I/Q data processing. I/Q data processing is used to determine if the return signal contains a detection. The processing done on this data is explained in *High Resolution Radar Cross Section Imaging* and *Fundamental of Radar Signal Processing* [45, 46] by D. Mensa and M. Richards, respectively. Recall that the representation of the return signal is in I/Q format, like eq. (2.26), meaning the input signal of the radar has a real and imaginary part. Knowing that the signal of the radar is a linear frequency modulated (LFM) waveform with a computer generated pseudo noise (PN) signal mixed into the transmitted signal is the key to finding the mathematical processes to interpret the data. Richards states that since the signal is an LFM, the resolution is increased beyond a simple pulse response by sweeping the instantaneous frequency over the desired range bandwidth contained in the pulse. Therefore, the signal is broken up into a linearly stepped frequency waveform.

$$x(t) = \sum_{m=0}^{M-1} x_p(t - mT) e^{j2\pi m \Delta F(t-mT)}, \tag{2.27}$$

where ΔF is the frequency step size, M is the number of slow time samples, T is the pulse repetition interval, $x_p(t)$ is the single pulse of the pulse train waveform, and t is time. However, the data components are in the frequency band; therefore, the equation takes on the following form:

$$V(f) = \sum_{n=1}^{N} a_n(t - nT)e^{jnr\frac{(t-nT)}{c}}, \tag{2.28}$$

where a_n is the scattering strength, f is the frequency constant, c is the speed or velocity of light constant, r is the current range, and N is the number of frequencies in the sweep. Mensa states in *High Resolution Radar Cross Section Imaging* [47] range distribution $a_n(r)$ is found by taking inverse Fourier transform (IFT),

$$a_n(\tau) = \sum_{k=1}^{K} V_k(f)e^{j2\pi\tau f}, \tag{2.29}$$

where $\tau = \frac{2r}{c}$ is the round trip delay and K is the number of complex pairs or range bins. The IFT comes with a resolution relationship. This is the range resolution of each complex pair. This relationship is:

$$B = \frac{c}{2\Delta r}, \tag{2.30}$$

and

$$L = \frac{c}{2\Delta f}, \tag{2.31}$$

where B is the frequency bandwidth of the sweep, L is the extent of the range profile, Δr is the range resolution, and Δf is the frequency resolution. This means that for every frequency sweep done at a range step, there is a complex output voltage recorded. When the inverse Fourier transform is performed on that set of frequency sweeps, the result is the range profile of the arena. This profile identifies the presence of distinguishable objects as part of the definition of range resolution. The range resolution is simply the ability to distinguish isolated scatters which are closely spaced together in range. According to eq. (2.30), it is easy to see that if the bandwidth of the signal is increased, the range resolution is improved, however, the range from eq. (2.31) decreases [48].

2.4.2 Radar Range Bin Response

The next two sections show the calculations used on the data from the radar measurement facility at NAWCWD that create a range profile of the test arenas. First, given a receiver complex voltage of the echo is proportional to the following equation:

$$r(t,f) = e^{j2ft\pi} \sum_{q=0}^{Q-1} \sqrt{\sigma_q} e^{-j2\pi R_q \frac{2f}{c}}, \tag{2.32}$$

where σ_q represents some relative voltage radar cross section which is proportional to the true power RCS of some discrete scatterer at a range of R_q, and f is the frequency, t is time, and c is the speed of light [49]. Now partition the ranges from the radar into discrete bins centered at R_i and δR wide for signal processing. Let $R_0 = 0$, which is located at the antenna aperture; thus $R_i = \delta R i = 0, 1, ...\infty$. The scatterers are separated into their respective bins:

$$r(t;f) = e^{j2\pi ft} \sum_{i=0}^{\infty} \sum_{q=R_i=(R-\frac{\delta R}{2}, R+\frac{\delta R}{2})} \sqrt{\sigma_q} e^{-j2\pi(2\frac{f}{c})R_q}. \tag{2.33}$$

Let $A[i]$ be the return from all scatterers in the ith range bin with the phase shift relative to the center of the range bin:

$$A[i] = \sum_{q=R_i=(R-\frac{\delta R}{2}, R+\frac{\delta R}{2})} \sqrt{\sigma_q} e^{-j2\pi(2\frac{f}{c})(R_i - R)}. \tag{2.34}$$

Equation (2.33) is now reduced to:

$$r(t;f) = \sum_{i=0}^{\infty} A[i] e^{j2f(t-\frac{2\delta R i}{c})}. \tag{2.35}$$

2.4.3 Pulsed Waveform and Stepped Frequency

Stepped-frequency radar sends out multiple pulses with each pulse at a different frequency. Defining a few terms will help analyze the return of stepped-frequency radar.

- $f_k = f_0 + \delta f k, k = 0, 1, K, N_s - 1$ are the frequencies in one sweep.

- f_0 is the frequency of the first step.
- δf if the frequency step width in Hz.
- N_s are the number of frequency steps per sweep.
- T_r is the receive pulse width.
- T_s is the fast time sampling interval.
- T_d is the time delay to the first sample.
- n is the number of samples.
- $P_T(t)$ is the pulse function.

The return form, the ith range bin, will have a duration of only T_r seconds if the pulse function s used to modulate the return from each range bin. Applying the pulse function to eq. (2.35) gives:

$$r(t;f) = e^{j2\pi ft} \sum_{i=0}^{\infty} A[i] e^{\frac{-j2f_k \delta R i}{c}} P_T(t - \frac{i2\delta R}{c}). \tag{2.36}$$

Demodulating the carrier will result in the following waveform sampled at $t = T_d + nT_s$:

$$y_n[k] = \sum_{i=0}^{\infty} A[i] e^{\frac{-j2f_k \delta R i}{c}} P_T(T_d + nT_s - \frac{i2\delta R}{c}). \tag{2.37}$$

By finding the values of i, the limits of the summation are simplified where, $P_T(T_d + nT_s - \frac{i2\delta R}{c})$ not equal 0 for fixed values of n:

- $0 \leq T_d + nT_S - \frac{i2\delta R}{c} \leq T_r$,
- $0 \geq \frac{i2\delta R}{c} - (T_d + nT_s) \geq -T_r$,
- $T_d + nT_s \geq \frac{i2\delta R}{c} \geq T_d + nT_s - T_r$,
- $\frac{(T_s + nT_s)c}{2\delta R} \geq i \geq \frac{(T_d + nT_s - T_r)c}{2\delta R}$.

Defining the ceiling and floor as u_n and v_n, respectively, so that $u_n = \frac{(T_d+nT_s-T_r)c}{2\delta R}$ and $v_n = \frac{(T_s+nT_s)c}{2\delta R}$. Adding this to eq. (2.37) results in:

$$y_n[k] = e^{-j2\pi f_k \delta R u_n \frac{2}{c}} \sum_{i=0}^{v_n-u_n} A[i+u_n] e^{-j2\pi f_0 \delta R i \frac{2}{c}} e^{-j2\pi \delta f \delta R i \frac{2}{c}}. \tag{2.38}$$

Equation (2.38) is almost in the form of a fast Fourier transform (FFT). Setting $\delta f \delta R \frac{2}{c} = \frac{1}{N_s}$, which defines the range resolution as $\delta R = \frac{c}{2\delta f N_s}$, the last exponential term in the summation becomes the FFT kernel. Setting the upper limit of the summation to $N_s - 1$ makes this an FFT. The conditions for doing this go as follows.

- For $v_n - u_n = N_s - 1$, the is no manipulation of the data.
- For $v_n - u_n \gg N_s - 1$, data is truncated along with the range profile.
- For $v_n - u_n \ll N_s - 1$, the data is padded with zeros, $A[i + u_n.] = 0$ for $i \gg (v_n - u_n.$

The final discrete waveform will be:

$$y_n[k] = e^{-j2\pi f_k \delta R u_n \frac{2}{c}} FFT[A[i+u_n] e^{-j2\pi f_0 \delta R i \frac{2}{c}}]. \tag{2.39}$$

The range profile is:

$$A[i+u_n] = e^{j2\pi f_0 \delta R u_n \frac{2}{c}} IFFT[y_n[k] e^{j2\pi f_k \delta R i \frac{2}{c}}], \tag{2.40}$$

where IFFT is the inverse fast Fourier transform.

2.5 Summary

Knowledge of the aperture and electromagnetic waves determine the amount of return signal reflected from an object. The return signal of echo gives information through demodulation of the signal. Processing of the I/Q data creates a range profile of the demodulated signal. This range profile shows where the targets exist down range.

Chapter 3

Presentation of Work Completed

This chapter highlights one of the many achievements of the GIF team at NAWCWD by showing the ability to determine the range resolution for a GIF and detect objects in the radar's field of view.

3.1 Radar Setup

The radar facility was readily available for limited use. The two major steps of the setup phase were to attach the pseudo-random bi-phase modulation radar to the transporter sled and connect the output of the radar to data acquisition devices. This may sound like an easy task, but radar testing is comprised of several devices. These include the antenna array, the digital signal processing computer, power supplies, signal filters, mixers, signal generators, a linear frequency modulator (LFM), and other devices. After the setup of the radar was complete, the task of programming the data acquisition devices and test controllers was done using LABView programming. LABView is an IEEE488-based visual programming language that can control each device, create data files, and send those files to the data acquisition computers.

3.1.1 New Hardware and Software Integration

Problems varied from recording the data incorrectly to testing work within operating parameters for twenty minutes and then retrogressing into bad data. Part of the problems occurred due to the age of the computer used to control the transporter. Documentation of the signals that the control computer uses was poorly written by the system designers. A controller was built to interface with these older systems. The controller used the LABView control program to route signal to the correct devices at the appropriate times. This resulted

in the ability to record the sled position, the range gate or range to target, and the signal measurements off the I/Q channels of the radar. The analysis of the I/Q data collected controller revealed test set issues and other unrelated software problems. Most importantly, the controller's data collection made it possible to determine the resolution of the radar to be high enough to detect targets in the resonance region.

3.1.2 Setup Issues

During the testing phase of the project, several more obstacles were found. One of the problems encountered was harmonic motion in the transporter sled. When the transporter moves, there are low frequency vibrations in the platform. These vibrations distort the high resolution data from the test. This was noticed during the first few test runs. To correct this problem, a high-pass filter was added into the data processing. The filter removes low harmonic frequency, such as sled movements, from the data. The filtered data was recorded and processing continued.

3.1.3 Component Breakdowns

A recurring problem during testing was radar breakdowns due to various components. These issues were found, tested, verified, and solved using microwave designing and sound engineering work. Other members of the GIF team made redesigns to the test set and ordered parts to fix any problems the radar or testing equipment had.

3.2 Data Processing

3.2.1 Software Issues

After calibration testing on the radar was performed, there was I/Q data available for processing. MATLAB was implemented to import the text files into manageable data columns. Each column of data represented a recorded data point such as the time, sled position, sled velocity, frequency, in-phase channel and quadrature-phase channel. MATLAB isolated the I/Q channels and performed a two column FFT on the data as described

in sec. 2.4.3. Creating the range profile by plotting data like in Appendix A.1 using the code in Appendix B.1 revealed flaws in the data. A noticeable data problem was partial frequency sweeps of a position at the beginning and end of the entire run. This was caused by a timing error between the controller and data recording devices. This data is deleted from the analysis. The next faulty points were the first two data points in each frequency sweep. These abnormal points were caused by settling in the receiver filters and are also removed from each sweep. The final data problem that was corrected in this phase of the project was an extra data point in the middle of some of the sweeps. The recorder simply added a copy of a data point in the middle of the run. All of the bad data points were removed by MATLAB code.

3.2.2 Range Profiles

The range profile does signify where the object is located down range for the radar at a fixed position. The resultant range profile plots in fig. 3.1 were made for a single trihedral and the triple trihedral arena. The maximum range of the triple trihedral arena is 512 bins and the single trihedral arena is 64 bins. The number of range bins are equal to a power of two, 2^N [50]. These numbers were chosen to enable the use of the fast Fourier transform on the data. The individual calculations for fig. 3.1 are in secs. 2.4.3 and 2.4.2. The range resolution of these figures can be found by going to eq. (2.30) and inputting the values for bandwidth $7GH_z$ and the speed of light. The range resolution for test run seven is therefore, $\Delta r = [1:N]\frac{c}{2Bm2in} = [1:512]\frac{30}{(2)(.7*8)(2.54)} \approx 1inch$ where N is the number of samples and $m2in$ is the conversion factor from meters to inches.

MATLAB generated fig. 3.1 which illustrates the full range profile of Run 14, a single trihedral arena with I/Q imbalances, and the full range profile of Run 7, a triple trihedral arena with I/Q imbalances. The MATLAB code for these plots is included in Appendix B.1. The single peak at $120dB$ in Run 14 identifies an individual trihedral in the range profile. In Run 7 the group of peaks at $125dB$ identify the triple trihedral group. The orientations of the trihedrals in this group are in a row. The threshhold for determining a target was not a set requirement of these test cases. Dr. Kidner did set a parameter for the

I/Q imbalances [51]. As seen in both plots in fig. 3.1, there are noticeable peak between range bin zero and the highest peaks in the range profile. These are the I/Q imbalances. The parameter for the imbalance was to have $25dB$ of difference between the highest peak in the profile and the noticeable imbalance. This parameter was met. The highest imbalance peaks are at $95dB$ for Run 14 and $100dB$ for Run 7. A noticeable difference between the two figure are the ranges and the resonant characteristics in Run 7. The data confirms that Run 7 was performed at a closer stationary position. This explains the resonant waves being more pronounced in the plot of Run 7. This completes the goal of determining a high range resolution for this GIF radar in the arena by identifying the object in the expected range gates.

3.3 Results

After looking at the range profiles of a test run in resonance region, the resonance from creeping wave going around an object can clearly be seen in fig. 3.1. However, there are distinguishable peaks that represent the objects in the arena. The same results would have been seen on a calibration sphere test. This raises the question on how to distinguish different types of objects. By increasing the bandwidth of the radar, one could effectively make a radar image of the object for identification. This will lower the effective range of the radar. Also, a trihedral was pointing directly at the radar making the return signal or scatter signal have a very high intensity, making the large spikes in the range profile. For a complex object, this may not necessarily be the case. There needs to be additional steps taken to complete the identification criteria of entire GIF project.

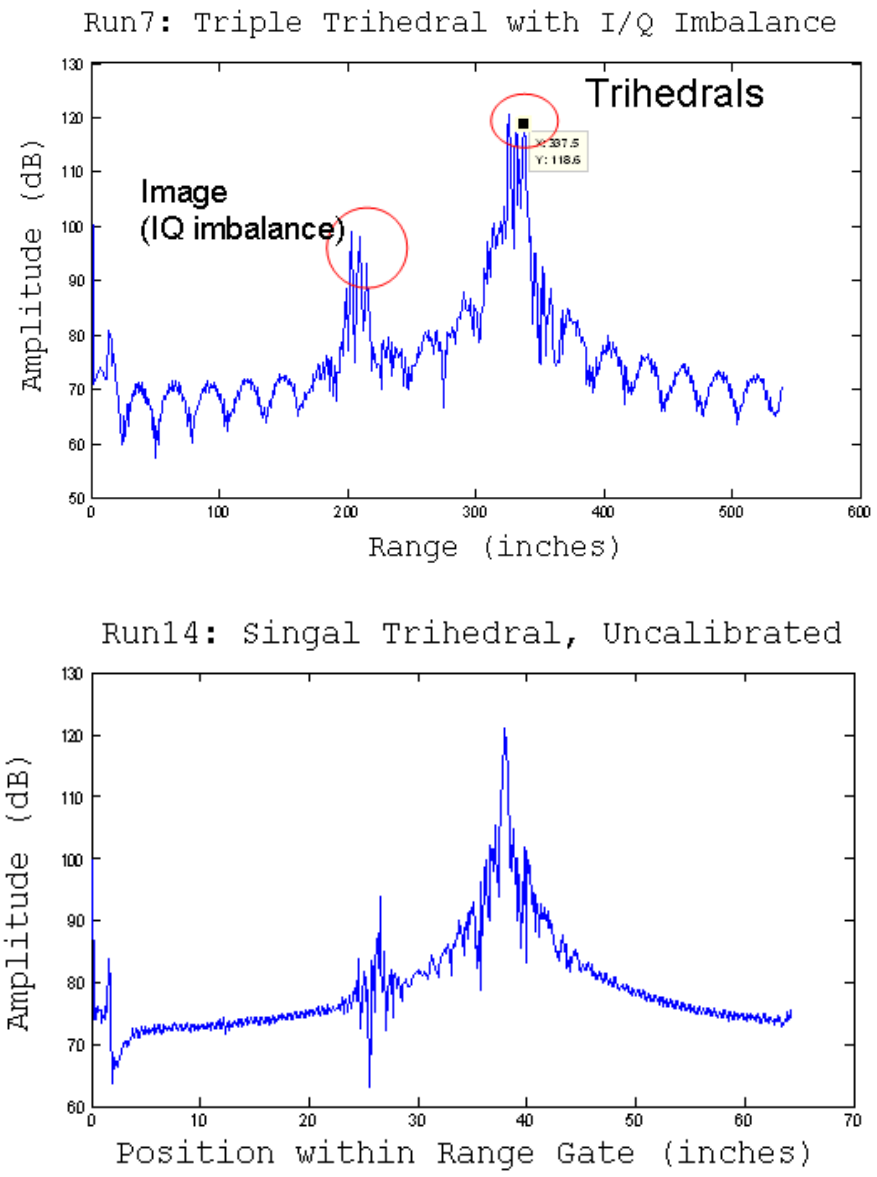

Fig. 3.1: Arena runs 7 and 14

Chapter 4

Conclusions

4.1 GIF Next Steps

A problem that was not correct in this part of the project was the I/Q imbalances in the range profile. This is currently being studied by other members of the GIF team. The processes they will use to eliminate these imbalances are as follows. First, analyze the frequency response of the I/Q data. The data should show three distinct signals, a DC component at the center frequency, a return signal from the object at frequency $+W$ and a reflection or mirror image at frequency $-W$. The final step will be to design a filter to eliminate the DC component and the reflection image. This will improve the ability to find object, eliminate the I/Q imbalance in the range profile and start taking steps to determine a threshold parameter for this radar.

Another project proposed has been to use a good ambiguity function that enhances match filter techniques on the signals. This will hopefully remove noisy scattering in the resonance region by reducing the presence of resonance waves in the data. When the ambiguity function is found, finding the exact shape and range of the object is possible due to the ability of programming a match filter dynamically. However, due to external factors, the analysis to find the ambiguity function of the radar will be postponed until a later date.

The project has taken a year and a half to get to this point. Additional problems were found in some of the data since receiving data from the calibration test. An error found in every other range bin has caused problems with data analysis. This problem has just recently been corrected, but not included in this paper.

4.2 Future Testing

There have been many promising strides in developing this type of guidance integrated

fuzing system. The fuze testing facility makes it possible to set up testing for missile projects and other military projects.

4.3 Possible Future Projects

Another possible project would be to put a complex target such as a tenth-scale Mooney 231 and compare it to the results of Jain and Patel [52,53]. This will validate the conclusion made in this paper and future work done on this project. This also creates additional work and a need to further study the resonance region of radar cross-section measurements of complex targets and build a database of complex objects for customers. After analysis of the radar cross-section measurements in the resonance region, this could lead to radar imagery in the resonance region. There are already techniques as explained in *High Resolution Radar Cross Section Imaging* and *Fundamental of Radar Signal Processing* [45, 46] for near-field applications. This type of application is valuable to customers who want to see radar imagery of an entire radar track going from far-field to resonance-field and finally to near-field.

4.4 Final Summary

The goal of finding the range resolution of the guidance integrated radar using specified mathematical techniques was accomplished. With the lessons learned and experience gain from this project, there now is a valuable asset that will continue to enhance weapons capabilities for many years to come.

References

[1] United States Navy, "NAWCWD." http://www.navair.navy.mil/nawcwd/index.html, Jan. 2009.

[2] The Ordnance Shop, "Missile Components." http://www.ordnance.org/missile_components.htm, 2008.

[3] P. H. Young, *Electronic Communication Techniques*, ch. 5, vol. 4, pp. 136-148, Upper Saddle River, NJ: Prentice Hall 1994.

[4] P. H. Young, *Electronic Communication Techniques*, ch. 9, vol. 4, pp. 313-370, Upper Saddle River, NJ: Prentice Hall 1994.

[5] S. Ghaleb, F. Schiavone, G. Roush and T. M. Fritz, "Acitve RF Seeker Guidance Integrated Fuzing." p. 4, Aug. 1995.

[6] W. G. Bath and G. V. Trunk, *Radar Handbook*, ch. 7, pp. 7.28-7.35, New York, NY: McGraw-Hill Companies, 2008.

[7] R. D. Cope, "Fuzing Overview." http://www.dtic.mil/ndia/44fuze/cope.pdf, 2007.

[8] S. Ghaleb, F. Schiavone, G. Roush and T. M. Fritz, "Acitve RF Seeker Guidance Integrated Fuzing." p. 3, Aug. 1995.

[9] M Skolnik, *Radar Handbook*, ch. 1, pp. 1.1-1.5 New York, NY: McGraw-Hill Companies, 2008.

[10] BBC, "The Secret War - vol. 1 - The Battle of the Beams / To See For A Hundred Miles," May 1994, film.

[11] E. F. Knott, *Radar Handbook*, ch. 14, p. 14.5. New York, NY: McGraw-Hill Companies, 2008.

[12] C. Uluisik, G. Cakir, M. Cakir, and L. Sevgi, "Radar cross section (RCS) modeling and simulation, part 1: a tutorial review of definitions, strategies, and canonical examples." *Antennas and Propagation*, vol. 50, num. 1, p. 117, Feb. 2008.

[13] S. Ramo, J. Whinnery, and T. Van Duzer, *Fields and Waves in Communications Electronics*, ch. 1, p. 8, New York, NY: John Wiley and Sons Inc., 2004.

[14] W. E. Blore, "The Radar Cross Section of Ogives, Double-Backed Cones, Double-Rounded Cones, and Cone Spheres." *Antennas and Propagation*, vol. 46, num. 5, pp. 582-590, Sept. 1964.

[15] A. S. Chen and E. K. Walton, "Comparison of Two Target Classification Techniques." *Aerospace and Electronic Systems*, vol. 22, num. 1, p. 21, Jan. 1986.

[16] A. S. Chen and E. K. Walton, "Comparison of Two Target Classification Techniques." *Aerospace and Electronic Systems*, vol. 22, num. 1, pp. 15-22, Jan. 1986.

[17] A. McCowen, J. A. R. Macnab and M. S. Towers, "Modelling the effectiveness of RAM coatings on PEC scatterers in the resonance region." *Antennas and Propagation*, vol.2, pp. 938-939, Feb. 1993.

[18] V. V. Veremey and R. Mittra, "Scattering from Structures Formed by Resonant Elements." *Antennas and Propagation*, vol. 46, num. 4, pp. 494-501, Apr. 1998.

[19] K. Chopper, H. Jaeger, L. Stephens, D. Burdic, C. Yang and C. F. Lin, "Seeker-Optimized Guidance Integrate Fuzing." in *Aerospace Control Systems* by IEEE, p. 559, May 1993.

[20] S. Ghaleb, F. Schiavone, G. Roush and T. M. Fritz, "Acitve RF Seeker Guidance Integrated Fuzing." Aug. 1995.

[21] K. Chopper, H. Jaeger, L. Stephens, D. Burdic, C. Yang and C. F. Lin, "Seeker-Optimized Guidance Integrate Fuzing." in *Aerospace Control Systems* by IEEE, pp. 559-562, May 1993.

[22] K. Chopper, H. Jaeger, L. Stephens, D. Burdic, C. Yang and C. F. Lin, "Guidance Integrated Fuzizng Anaylsis and Simulation." *Control Applications*, vol. 2, pp. 750-755, Sept. 1992.

[23] Z. Wang, W. Li and N. Fan, "Integration of Guidance and Fuze of Directional Warhead Missile." *International Journal of Mathematics and Computers in Simulation*, vol. 1, num. 4, pp. 333-337, July 2007.

[24] C. Kidner and C. Tonks, "Talk about Guidance Integrate Fuze." Aug. 2008, interview.

[25] C. A. Balanis, *Antenna Theory*, ch. 1, p. 1, New York, NY: John Wiley and Sons Inc., 1982.

[26] D. J. Baker, *Maxwell's Equations for Electrmagnetics*, ch. 1, pp. 4-6, Logan, UT: Utah State University, 2006.

[27] C. A. Balanis, *Antenna Theory*, ch. Table of Contents, p. viii, New York, NY: John Wiley and Sons Inc., 1982.

[28] C. A. Balanis, *Antenna Theory*, ch. 2, p. 25, New York, NY: John Wiley and Sons Inc., 1982.

[29] C. A. Balanis, *Antenna Theory*, ch. 2, pp. 27-28, New York, NY: John Wiley and Sons Inc., 1982.

[30] C. A. Balanis, *Antenna Theory*, ch. 2, p. 29, New York, NY: John Wiley and Sons Inc., 1982.

[31] S. Ramo, J. Whinnery, and T. Van Duzer, *Fields and Waves in Communications Electronics*, ch. 1, p. 8, New York, NY: John Wiley and Sons Inc., 2004.

[32] P. L. Werner, A. J. Ferraro, D. H. Werner, *Electromagnetic Fields*, ch. 16, pp. 16.11-16.12 Danvers, MA: CRC Press LLC., 2002.

[33] C. A. Balanis, *Antenna Theory*, ch. 2, pp. 44-46, New York, NY: John Wiley and Sons Inc., 1982.

[34] A. Peterson, R. Mittra and S. Ray, *Computational Methods for Electromagnetics*, ch. 2, pp. 38-39, New York, NY: IEEE Press, 1998.

[35] P. L. Werner, A. J. Ferraro, D. H. Werner, *Electromagnetic Fields*, ch. 16, p. 16.9 Danvers, MA: CRC Press LLC., 2002.

[36] C. A. Balanis, *Antenna Theory*, ch. 2, p. 43, New York, NY: John Wiley and Sons Inc., 1982.

[37] E. Hecht, *Optics*, ch. 4, p. 96, San Francisco, CA: Addison Wesly, 2002.

[38] A. Peterson, R. Mittra and S. Ray, *Computational Methods for Electromagnetics*, ch. 1, pp. 24-28, New York, NY: IEEE Press, 1998.

[39] C. A. Balanis, *Antenna Theory*, ch. 2, pp. 65-66, New York, NY: John Wiley and Sons Inc., 1982.

[40] E. F. Knott, *Radar Handbook*, ch. 14, pp. 14.1-14.5. New York, NY: McGraw-Hill Companies, 2008.

[41] C. A. Balanis, *Antenna Theory*, ch. 2, p. 64, New York, NY: John Wiley and Sons Inc., 1982.

[42] L. Wilkerson, W. Carter, N. Schmidt and H. Franz, "Electronic Warfare and Radar System Engineering Handbook." Apr. 1997, NAWCWPNS TP 8347, http: ewhdbks.mugu.navy.mil.

[43] M. E. Yeomans, *Radar Handbook*, ch. 6, p. 6.33, New York, NY: McGraw-Hill Companies, 2008.

[44] M. E. Yeomans, *Radar Handbook*, ch. 6, pp. 6.31-6.36, New York, NY: McGraw-Hill Companies, 2008.

[45] M. A. Richards, *Fundamental of Radar Signal Processing*, ch. 4, pp. 205-223, New York, NY: McGraw-Hill Companies, 2005.

[46] D. L. Mensa, *High Resolution Radar Cross Section Imaging*, ch. 3, pp. 47-83. Norwood, MA: Artech House, 1991.

[47] D. L. Mensa, *High Resolution Radar Cross Section Imaging*, ch. 3, p. 47. Norwood, MA: Artech House, 1991.

[48] D. L. Mensa, *High Resolution Radar Cross Section Imaging*, ch. 3, p. 49. Norwood, MA: Artech House, 1991.

[49] S. Neilsen, "Stepped Frquency Range Profile Calculation," NAWCWD, Apr. 2008.

[50] M. I. Skolnik, *Introduction to Radar Systems*, ch. 3, p. 141. New York, NY: McGraw-Hill Companies, Inc. 2001.

[51] C. Kidner and C. Tonks, "Talk about Guidance Integrate Fuze Testing." Dec. 2008, interview.

[52] A. Jain and I. Patel, "Ground-to-air imaging radar for RCS measurement." *Instrumentation and Measurement*, vol. 41, num. 6, pp. 951-956, Dec. 1992.

[53] A. Jain and I. Patel,"Dynamic imaging and RCS measurements of aircraft." *Aerospace and Electronic Systems*, vol. 31, num. 1, pp. 211-226, Jan. 1995.

Appendices

Appendix A

I/Q Data

A.1 I/Q Data Table of A/D Channels 1 and 9

Table A.1 is a table of channels 1 and 9 the raw data of the I/Q components required to make a complex pair. These complex pairs will have the inverse Fourier transform performed on them in order to determine the range resolution.

Table A.1: Sample data from output file of LABView Control Program.

$Channel_1$	$Channel_9$
-1527	352
-914	936
-112	802
316	101
96	-1755
-622	-935
-1310	-607
-1544	140
-1199	794

Appendix B

I/Q Data Analysis

B.1 MATLAB Code Used to Break-up Raw Data and Perform IFT

This is the MATLAB Code that created the plots in fig. 3.1. A complete output file, namely run7.txt or run14.txt, are required for this script to function properly.

```
fp=fopen('run7.txt');
%Open the file run7.txt or run14.txt
C=textscan(fp,'%d32','Headerlines',1);
%All of the data is put in one very long vector
dat=reshape(C{1,1},19,[]);
%Each row is the data out of one data channel
reflect=(double(dat(1,:))+j*double(dat(9,:)));
%Range gate 1 is in A/D channels 1 (I) and 9 (Q)
reflect(:,47055:end)=[];
%Delete the partial sweep at the end of the file
reflect(:,36814:41934)=[];
%Delete the sweep with an extra data point in the middle of the file
reflect(:,1:973)=[];
%Delete the partial data run at the beginning of the file
reflect2=reshape(reflect,10,[]);
%Each column is a frequency hold (10 samples)
reflect2(1:2,:)=[];
%Delete the portion of the sweep in which the filters are settling
ref_av=mean(reflect2);
```

```
%Average the data in each frequency hold
ref_av2=reshape(ref_av,512,[]).';
%Each column is now the same frequency point in different sweeps:
%each row is a different sweep
ref_av2(4:6,:)=[];
%Delete the phase corrupted data in the middle of the run
reflect7=mean(ref_av2);
%Average the data over the remaining sweeps
time_domain=fft(reflect7);
%Convert to the time domain
x_scale=[1:512]*30/(.7*8)/2.54/2;
%Create the proper time scale
plot(x_scale,20*log10(abs(time_domain)))
%Plot the data
```